DeLiDAR: Decoupling LiDARs for Pervasive Spatial Computing

Darshana Rathnayake
Singapore Management University
Singapore
darshanakg.2021@phdcs.smu.edu.sg

Razat Sutradhar
Georgia State University
Atlanta, GA, US
rsutradhar1@student.gsu.edu

Abbaas Alif Mohamed Nishar
Georgia State University
Atlanta, GA, US
amohamednishar1@student.gsu.edu

Dulaj Sanjaya Weerakoon
Singapore-MIT Alliance for Research and Technology
Singapore
dulaj.weerakoon@smart.mit.edu

Ashwin Ashok
Georgia State University
Atlanta, GA, US
aashok@gsu.edu

Archan Misra
Singapore Management University
Singapore
archanm@smu.edu.sg

Abstract

Unbounded proliferation of LiDAR-equipped pervasive devices generates two challenges: (a) mutual interference among emitters and (b) significantly higher sensing energy overhead. We propose a fundamentally different approach for LiDAR sensing, in indoor spaces, that decouples the sensor's emitter and receiver components. Our proposed approach, called *DeLiDAR*, centralizes the emitter functionality in one or more stationary nodes that continually emit pulses; this decoupling allows each mobile LiDAR sensor to be an ultra-low power, pure receiver unit consisting solely of passive multiple photodiodes. We explain how the emitter can utilize VLC-based encoding of its pulses to convey parameter settings that allow a receiver device to infer its own point cloud, without requiring any timing or clock synchronization with the emitter. An initial experimental setup, consisting of a Raspberry Pi and an Arduino-based emitter/2-diode receiver, demonstrates the ability to recover the light pulse's AoA with a resolution of ±5°. We also highlight key systems challenges to realize *DeLiDAR* in practice.

CCS Concepts

• **Hardware** → *Sensors and actuators.*

Keywords

LiDAR, Depth estimation, Angle of Arrival estimation

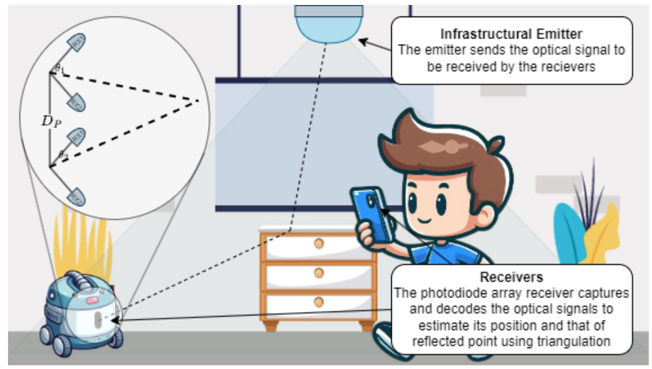

Figure 1: The Decoupled LiDAR Concept

1 Introduction

Originally spurred by the goal of providing 3D situational awareness to autonomous vehicles, LiDAR (light detection and ranging) sensors have now become a mainstay for supporting spatial sensing and computing across many mobile, wearable and IoT devices. They are embedded in smartphones to support augmented reality (AR) applications, smart glasses for advanced spatial computing, and home cleaning robots for autonomous navigation around obstacles. LiDARs function by emitting a beam of light that reflects back to a receiver (photodiode), measuring the time-of-flight (ToF).

However, the wider adoption of LiDAR sensing in mobile and wearable devices gives rise to two challenges: mutual interference and high power consumption. When multiple LiDARs simultaneously scan the same physical environment, interference occurs because one receiver may pick up the reflection of a beam from another LiDAR's emitter, corrupting its ToF calculation. LiDARs also consume significantly more power due to the energy required to continuously emit the light beam. Our research is motivated by the question: *is it possible to reposition LiDAR as a lower-power, ubiquitous sensor for future mobile, wearable, and IoT devices, with multiple LiDAR sensors operating blithely in a collocated environment?*

Proposed *DeLiDAR* approach. We believe these challenges can be answered affirmatively by adapting the bistatic configuration for LiDARs. Specifically, we propose *disaggregating* the transmit/emit and receive functions of a LiDAR and placing them in different devices. Figure 1 illustrates the core concept of our Decoupled LiDAR framework, called *DeLiDAR*. An infrastructure-mounted light emitter (source) actively generates light pulses that are reflected by various objects in the environment, while the mobile/embedded "sensors" consist of an array of photodiodes that passively receive these reflections. The fundamental idea is to use a common emitter that continuously beams packets with timing, identity, and location (position coordinates) information across the space. Each emitted optical beam reflects off points in the environment and is detected by the passive receivers. The receiver uses the optical signal strength on the photodiode array to estimate the angle-of-arrival (AoA) and hence the position of the reflection point. The receiver then decodes the packet information to estimate the emitter's position and that of the reflection point relative to the emitter.

Benefits of *DeLiDAR*. The benefits of centralizing the emitter in a single, stationary infrastructure device are twofold: (a) it eliminates the power-hungry component of a traditional LiDAR, simplifying the mobile/IoT embedded LiDAR sensor into a set of photodiode “receivers“ with low-power consumption, and (b) it addresses the interference challenge by avoiding the contention caused by uncoordinated emissions from multiple light emitters. However, one might naturally question how the receivers can estimate depth through ToF calculation without knowing the exact time and location of the emitted pulses. Existing LiDARs estimate depth using various techniques (e.g., direct and indirect ToF, frequency-modulated continuous-wave (FMCW), amplitude-modulated continuous wave (AMCW)), which intrinsically assume a tight clock or signal synchronization between the emitter and receiver. Such synchronization is patently infeasible for the decentralized and independent operation of receivers and emitters. We show that this challenge can also be overcome without any clock synchronization, by combining known techniques of visible light communication (VLC) with LiDAR-ranging–i.e., by effectively encoding appropriate parameters of the emitter's operation within the emitter light pulses. The key to our uncoordinated operation is the use of *multiple photodiodes* (photodiode arrays) on each receiver unit. By combining (a) known models of photodiode current strength variation as a function of angle of incidence [2] with (b) angle-of-arrival (AoA) estimation approaches popularized by multi-element wireless antennas [10] to triangulate the reflection point in the environment, the receivers can reconstruct their egocentric point cloud. We show that: (a) If the IoT/wearable device only needs to estimate an egocentric point cloud (i.e., depth estimates of the environment relative to its location), it can estimate the distance to a reflected point via AoA estimation and triangulation. (b) If the IoT/wearable device wants to establish its view of the point cloud (and its location) in a global coordinate system, we can use VLC techniques to embed the emitter's location coordinate information within the emitter pulses.

The key contributions of the paper are:

(1) We introduce the concept of bistatic/decoupled LiDAR, which differs from the universally accepted monostatic configuration. Instead, in *DeLiDAR*, the emitter's function is a core ‘infrastructure service’ to wearable/IoT nodes that wish to perform LiDAR-based ranging of their environment, and the LiDAR ‘sensor’ hardware then simplified to a set of low-power and inexpensive photodiodes.

(2) We demonstrate how to use VLC encoding on emitted pulses, enabling the emitter and receiver devices to operate independently. We show how the *DeLiDAR* paradigm allows receiver devices to estimate an egocentric point cloud by performing AoA-based ranging with photodiode-based receivers. Additionally, we encode the emitter's location and pose of emission into the pulses to localize the receivers in a global coordinate system.

(3) We use a rudimentary but functional implementation to demonstrate the validity of the proposed *DeLiDAR* concept. We design and validate the AoA concept in 2D over a 10 cm range using a single infrared emitter and a two-element photodiode receiver. We demonstrate (a) AoA estimation using the ratio of received signal strength of the reflected beam on two photodiodes, and (b) the successful communication and decoding of VLC packets. We conduct our exploration in the infrared (IR) wavelength to consistently emulate typical LiDARs and to remain unobtrusive.

(4) We also enumerate the open challenges associated with realizing the *DeLiDAR* paradigm. These include the need to (a) install and coordinate multiple emitters within a single instrumented indoor space to overcome range-vs.-resolution loss, and (b) tune the VLC-encoded content to balance the tradeoff between *DeLiDAR's* goals of finer spatial resolution and high scanning frequency.

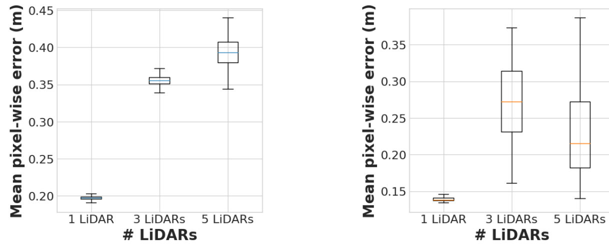

(a) Intel L515 (b) ArduCam ToF

Figure 2: Impact of multi-LiDAR interference

2 LiDAR Background and Challenges

A LiDAR typically consists of an emitter collocated with a single-photon avalanche detector (SPAD) receiver. The emitter beams a pulsed laser for an extremely short period, on the order of a few picoseconds to nanoseconds. The SPAD receiver detects only the first arriving photon of these emissions after reflecting from a point in space. In this way, SPAD can rule out noise from other sources based on the low probability of competing photons arriving within the ultra-short time window. The emission and reception functions are triggered almost instantaneously to estimate the distance using the ToF method. While the monostatic structure of today's LiDARs is its strength, it also presents two challenges that become more pronounced as LiDARs are embedded in a wider variety of mobile, wearable, and IoT devices: interference from other LiDARs and high energy overhead. Before discussing how our proposed *DeLiDAR* approach addresses these issues, we first explore these challenges in more detail.

Interference. There are two categories of interference: direct and indirect, depending on how the foreign laser pulses are received by a LiDAR. Direct interference occurs when a LiDAR receives another LiDAR's direct transmission, while indirect interference occurs when it receives reflected laser pulses. We assess the impact of interference on two different LiDARs, Intel L515 and ArduCam ToF, in a static environment with varying numbers of concurrent LiDARs: 1 (no interference), 3, and 5 LiDARs. We obtain a reference frame for each LiDAR by pixel-wise averaging a sequence of depth images captured without interference. The error is reported by averaging the absolute differences between the reference frame and each interfered frame in a sequence. The error with no interference is known as the random error. We observed random errors of 20 cm for the Intel L515 and 13 cm for the ArduCam ToF. The errors increased and/or exhibited significant variation as the number of LiDARs increased as shown in Figure 2.

Energy. Due to its active nature, LiDAR's high power consumption poses a challenge, especially for battery-powered mobile and wearable devices. We measured the power consumption of three different LiDAR sensors: Intel L515 (4.6 W), Azure Kinect DK (2.3 W), and ArduCam ToF (1.7 W). These measurements include the

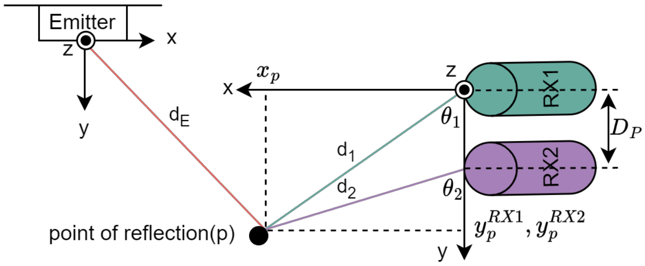

Figure 3: The placement of the Emitter (E), Receiver (Rx), and Point of Reflection (p). Each node has its {X, Y, Z} axes of reference. A receiver-device contains multiple receivers (RX$_i$s) translated by a known distance of D_P; with each RX$_i$ comprising photodiode pairs across the 3D orthogonal planes.

power consumed for on-device processing to estimate depth using raw data. It is evident that LiDARs consume substantially more power compared to alternative sensors (e.g., inertial sensors) on mobile devices, which consume around 100 mW. We also separately measured the power consumption of the IR emitter and receiver and observed that *the emitter consumes the overwhelming percentage of power*, due to its need to generate, amplify, and transmit the photon pulses. Not including the microcomputer ON power draw, the basic power budget to keep one LED ON at the highest range was 2.2 Watts (1A at 2.2V input); in contrast, the 'receiver' photodiode does not need to draw any current for detecting the signal (and generates photo-current upon signal reception).

3 Proposed Decoupled LiDAR

The crux of the proposed *DeLiDAR* paradigm, that differentiates from monostatic LiDARs, is the physical separation of the optical emitter from the receiver. For ease of exposition, we consider an IR-based LiDAR for our preliminary explorations.

Infrastructure as a Service Light Emitter. The *DeLiDAR* system consists of an emitter strategically placed in a room where LiDAR imaging is required. The emitter should cover the entirety of the room space by adjusting its power. If the emitter cannot reach the farthest point in the room due to power limitations or the large size of the room, multiple emitters can be installed. Moreover, the emitters are expected to be part of the infrastructure with access to the power supply and a low-latency network medium (ethernet or nearest wireless access point). The number of diodes on the emitter will depend on the volumetric area of the space to be covered and will likely need to be arranged in a full or hemispherical fashion to cover the space. A common microcontroller on each emitter will control each diode. Protocols such as time/space division multiplexing will be experimented with to find the optimal firing sequence of the diodes in the emitter. The emitter will encode each transmission with information such as its angular position and timestamp using techniques in optical wireless communication, e.g., ON-OFF Keying (OOK), where a high state of the pulse represents bit '1' and a low or zero state of the pulse represents bit '0'. The fundamental requirement, however, is to ensure that these emissions from each diode are fast enough, similar to LiDARs, to minimize interference from other potential emitters and avoid adding latency to the real-time point cloud estimation process.

Low-power Optical Receiver. The receiver comprises an array of photodiodes, strategically arranged, e.g., on a hemisphere, to receive the reflected optical beams from various angles in the room. Considering the three 2D planes that cut across a 3D point coordinate of interest, we posit that it is possible to estimate AoA over each of the 2D planes using a *single pair of photodiodes* arranged over that plane. Consider a single 2D place (say parallel to the ground) and that the height from the ground is fixed. We can then use two photodiodes oriented away from each other with a known angle of separation (say δ). Prior work [2] has demonstrated how the angle of arrival (say θ) for each photodiode in the 2D plane can be estimated by using the Lambertian fall off in photoreceptor optical intensity: the current generated on the photodiode is proportional to the *cosine* function of angle of arrival. In this way, the angle of arrival on each of the three 2D planes can be estimated using the *ratio of signal strength on each pair of photodiode* along each plane. By using the knowledge of the known distance between each photodiode pair receptors, we can then compute the (x,y,z) coordinates of the point of reflection with respect to the receiver. The timing and position coordinated encoded in the VLC packet from the emitter will be used to estimate the distance between the emitter and the point of reflection. Thus, the (x,y,z) coordinates with respect to the emitter or a global reference frame, can also be computed. For example, in Figure 3, RX1 and RX2 represent a 2-element photodiode array separated by an angle δ, and these pairs are separated by a distance D_P along their *base* plane. With knowledge of θ_1, θ_2, and D_P, the distance along vectors d_1 and d_2 can be computed. Subsequently, using the VLC packet information, d_E can be estimated.

4 Preliminary Exploration

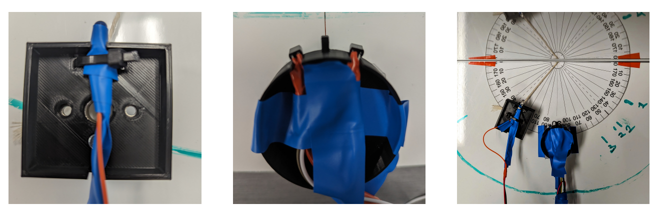

(a) Single-element LED emitter **(b) 2-photodiode optical receiver** **(c) Our experimental setup**

Pilot Code (14 bits)	Barker Code (5 bits)	Timestamp (64 bits)	X Coordinate (16 bits)	Y Coordinate (16 bits)	Y Coordinate (16 bits)	ID (16 bits)	Barker Code (3 bits)	Angle (9 bits)	CRC (8 bits)	Stop Code (8 bits)

(d) Emitter packet structure used for VLC

Figure 4: The setup for *DeLiDAR* preliminary feasibility experiments, following NEC IR remote standards.

We demonstrate the feasibility of estimating the coordinates of a reflected point using our proposed *DeLiDAR* concept. To this end, we set up ourselves for estimating AoA in a 2D setup using a single LED emitter and a two-photodiodes receiver (see Figure 4). Both, the emitter and receiver were controlled using an Arduino Mega for optical pulse emission and detection (and conversion to digital values). A Raspberry Pi4 is also interfaced with the emitter and receiver. The photodiode pair was rotated with an angle $\delta = 45$ deg (±22.5deg separation centered at 0). The VLC packet size is 149 bits and the transmitted ON-OFF Keying pulse duration was 1 msec, with photodiodes sampling at 2x transmit rate (every 0.5ms) following Nyquist criterion. All measurement collections were repeated five times, and the average is reported. The measured packet error rate in our measurements is less than 5%.

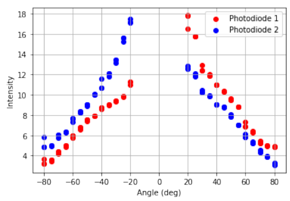

(a) Raw Intensity Measurements

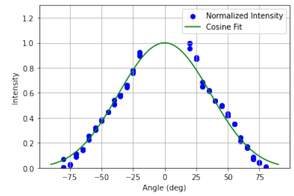

(b) Lambertian Response Validation

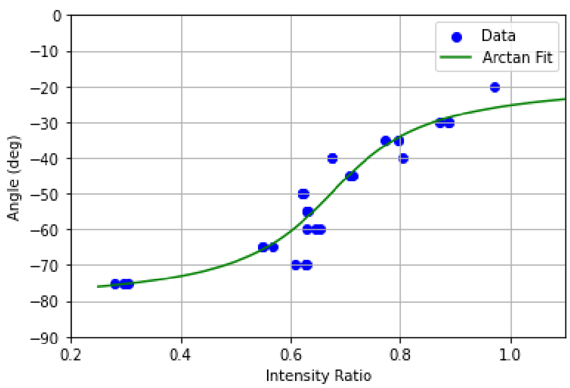

(c) AoA vs the photodiodes intensity ratio ($\frac{PD_1}{PD_2}$).

Figure 5: Photodiode intensity-Based AoA Estimation

We plot the photodiode intensity readings vs. the angle of reception or arrival (θ) of the reflected ray (angle between LED emitter normal and receiver normal that bisects the photodiode pair) in Figure 5a. (We excluded the readings between -20° and 20° as they were determined to be faulty due to wiring issues.) Upon curve-fitting the photodiode intensity behavior we observe a good fit (Figure 5b) with a $\cos^n(\theta)$, where $n = 9$. This conforms well with Lambertian theory of photodiode reception intensity fall off being proportional to $\cos^n(\theta)$ where $n = \frac{-\ln(2)}{\ln(\cos(\theta_{1/2}))}$, where $\theta_{1/2}$ is the photodiode reception half-angle (angle of reception where photodiode detected intensity is half that of at maximum, at 0 degree). In our experiments, this was 25 deg, which results in $n = 8.7$. In fact, we find that the exact curve-fit was $a\cos^9(b\theta)$, where $a = 1, b = \frac{1}{107.98}$.

We use the cosine relationship between photodiode intensity and its AoA, to derive an expression to compute the AoA. In Figure 5b, the photodiode received signal strength values are normalized to visualize the relationship (curve-fit) better. As such it is not possible to directly compute the AoA from a single photodiode reading without knowing the exact multiplicative and additive scalars involved in the $\cos^9(\theta)$ function. However, consider the ratio of the photodiodes,

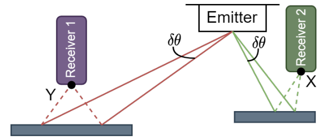

(a) A scenario where spatial resolution varies with the positioning of the receivers.

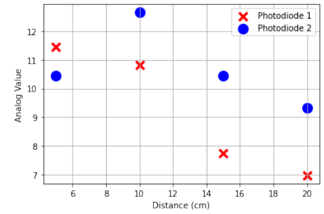

(b) Photodiodes' intensity at the same AoA (45°) with varying distance to the emitter.

Figure 6: Spatial resolution variation with receiver positioning

$$r = \frac{PD_1}{PD_2} = \frac{\cos^9(b\theta + b\frac{\delta}{2})}{\cos^9(b\theta - b\frac{\delta}{2})} \tag{1}$$

This is solvable and results in a closed-form expression for AoA as an inverse tangent function of intensity ratio r [2] as,

$$\theta = \frac{1}{b}\arctan\{\frac{1}{\tan(0.5b\delta)}[\frac{r^{1/9}-1}{r^{1/9}+1}]\} \tag{2}$$

Using numerical methods we find the relationship between ground-truth θ and the r computed using measurements as, $\theta = 20.58 * arctan(7.72 * r - 5.21) - 49.83$, as shown in Figure 5c. Upon validation check, we observe an average of ±5° and a maximum of ±10° in AoA estimation using our ratio-based approach for our measurement dataset. Computing the ratio between the photodiodes' intensity and AoA is a one-time calibration process for a choice of photodiodes. This calibration is independent of the environment and can be done apriori.

4.1 Limitations and Research Challenges

Location-dependent Spatial Resolution: Conventional LiDARs exhibit a range-dependent spatial resolution. Specifically, as a unit angular change in the emitter direction results in a wider spatial change at longer distances, LiDAR-generated point clouds are typically denser, with finer resolution, for points closer to the sensor than points farther away. For LiDARs embedded in mobile devices, this variation is usually acceptable because of the higher saliency for proximate points–e.g., a vehicle needs finer-grained spatial knowledge for proximate vs. farther objects. In *DeLiDAR*, this behavior can lead to an unfortunate artifact: the spatial resolution now depends on the position of objects in environment *relative to the emitter, rather than the receiver*. Consequently, if a mobile device finds itself at a point (illustrated in Figure 6) Y where the emitter signal is reflected off a more distant surface compared to another location X, its computed point cloud will be coarser for points nearer to Y. If not rectified, this can lead to an unsatisfactory user experience with various spatial computing applications. We believe that this issue can be addressed by suitably instrumenting the environment with *multiple* emitters, spatially distributed to assure multiple redundant receiver signals for any specific real-world location.

Coordination among Multiple Emitters: To make *DeLiDAR* a reality, we need to deploy multiple static emitters, both to assure coverage (individual emitters are typically range-constrained due to regulatory power restrictions) and overcome the location-dependent resolution issue mentioned above. These emitters can be centrally controlled to avoid mutual interference–e.g., by time-multiplexing their emissions to avoid overlap [4]. Any such multi-sensor deployment will see a tradeoff between a single emitter's duty cycle and the number of concurrent emitters–larger the number of emitters, the longer the gap between consecutive active probing periods of an individual emitter. This phenomenon effectively translates into a tradeoff between the *quality* of the emitter infrastructure (the larger the number of emitters, the more accurate and robust the point cloud construction) and the *frequency* of point cloud generation (lower the number of emitters, the higher the frequency of probing by an individual emitter). To balance these objectives in a practical *DeLiDAR* deployment, we must develop an appropriate method to compute the *number & location* of emitters.

VLC signal length vs. LiDAR responsiveness: *DeLiDAR* utilizes VLC to encode a unique pulse ID and emitter ID, as well as additional emitter (location, pose) information (if absolute localization is desired). In general, including more information in the VLC channel increases the duration of a single pulse, which leads to a lower temporal frequency of LiDAR-based sampling. In our feasibility analysis, the packet size was 149 bits with a transmit rate of 1Kbits/sec, and this takes close to 400ms to estimate one point cloud from the single LED - single pair photodiodes setup (about 200ms each on TX and RX). While this duration can also be reduced by using more efficient VLC modulation techniques (e.g., pulse position modulation (PPM) for ultra-short duration pulses), higher symbol density in modulation typically has a lower SNR implying greater susceptibility to external lighting artifacts. The *DeLiDAR* system must thus be carefully designed to balance the accuracy-vs.-range tradeoff arising from these phenomena.

5 Related Works

Bistatic RADARs utilize two separate antennas for transmission and reception, situated at considerable distances from each other. Unlike monostatic RADARs, they require solving the transmitter-target-receiver triangle, known as the bistatic triangle. The MIMO concept, introduced in [11], measures the distance to the target by calculating 2D angles with an array of receivers, eliminating the need for synchronization in bistatic RADARs. The bistatic configuration has been explored for LiDARs, primarily for aerosol profiling [3]. LiDAL [1] has discussed the separation of transmitter and receiver for indoor detection and localization of individuals, relying on their mobility to distinguish them from background objects. However, the use of decoupled LiDAR for 3D indoor reconstruction remains unexplored in the literature.

The telecommunication theory's applicability to mitigating LiDAR interference was discussed in [4]. Wavelength-Division Multiple Access (WDMA) stands out as an effective approach that does not necessitate centralized coordination among sensors. However, it is important to note that the number of available channels within the operational spectrum is constrained by the regulations related to eye safety. Spatio-temporal filtering methods such as [7] have been proposed to recognize the interfered points in point clouds. These methods do not focus on recovery from such interference and often impose a computational burden. Several studies have been conducted to demonstrate the impact of interference [5] on different LiDAR sensors, and have proposed different techniques to mitigate the interference. A variable random delay is applied to the laser pulses generated by a time-correlated single-photon counting (TCSPC) LiDAR in [4]. The inability to predict the emission time of laser pulses makes this approach robust to interference. Kim et al. [8] proposed a new pulsed scanning LiDAR by modulating the pulses to include a unique device number, location of the pixel, and checksum. Nevertheless, the introduction of additional hardware components for modulation, the extension of pulse durations, and the integration of post-processing algorithms [6] would result in further escalation of power consumption.

The VLC community has extensively conducted research on positioning. Works such as LiSense [9] have also demonstrated the ability to detect human gestures/action under a multiple-input multiple-output ceiling LED and floor Photodiode array setup in a room. The work in [12] presents a design for indoor localization using a radio and VLC hybrid setup. Unlike our proposed *DeLiDAR* system these prior works do not achieve 3D mapping in a truly mobile setting.

6 Conclusion

Through the vision for *DeLiDAR*, we have argued how the separation of emitter and receiver for LiDAR functionality, allows the emitter to be developed as a stationary, infrastructure-based enabler for 3D point cloud sensing and, in turn, transforms the mobile/IoT device-based LiDAR component to one that performs pure passive photo-diode based sensing. We have theorized and used a simple preliminary hardware prototype to demonstrate (a) how VLC-based modulation can be used to encode relevant emitter information in a generated light pulse (1 ms duration), and how such information can be combined with spatial models of photo-diode current intensity to infer the reflected points in the environment with AoA error of $\pm 5^\circ$. These are, of course, preliminary numbers with low-end, proof-of-concept hardware; system performance can be significantly improved with the use of a larger array of photo-diode receivers and faster VLC-encoded pulse generation. We believe that implementing this de-coupled framework will allow fine-grained, low-power spatial awareness to be available across a much wider array of mobile and IoT devices.

Acknowledgments

This work was supported by (a) the National Research Foundation, Prime Minister's Office, Singapore, through its NRF Investigatorship grant (NRF-NRFI05-2019-0007) and the Campus for Research Excellence and Technological Enterprise (CREATE) program, and (b) the National Science Foundation under Grant No. NSF CAREER CNS-2146267. The Mens, Manus, and Machina (M3S) is an interdisciplinary research group (IRG) of the Singapore MIT Alliance for Research and Technology (SMART) centre. Any opinions, findings, conclusions, or recommendations expressed in this material are those of the author(s) and do not reflect the views of National Research Foundation, Singapore.

References

[1] Aubida A Al-Hameed, Safwan Hafeedh Younus, Ahmed Taha Hussein, Mohammed Thamer Alresheed, and Jaafar MH Elmirghani. 2019. LiDAL: Light detection and localization. *Ieee Access* 7 (2019), 85645–85687.

[2] Ashwin Ashok, Chenren Xu, Tam Vu, Marco Gruteser, Rich Howard, Yanyong Zhang, Narayan Mandayam, Wenjia Yuan, and Kristin Dana. 2016. What Am I Looking At? Low-Power Radio-Optical Beacons for In-View Recognition on Smart-Glass. *IEEE Transactions on Mobile Computing* 15, 12 (2016), 3185–3199.

[3] John E Barnes, NC Parikh Sharma, and Trevor B Kaplan. 2007. Atmospheric aerosol profiling with a bistatic imaging lidar system. *Applied optics* 46, 15 (2007), 2922–2929.

[4] Lucio Carrara and Adrian Fiergolski. 2019. An Optical Interference Suppression Scheme for TCSPC Flash LiDAR Imagers. *Applied Sciences* 9, 11 (Jan. 2019), 2206.

[5] Jeongsook Eom, Gunzung Kim, and Yongwan Park. 2019. Mutual interference potential and impact of scanning lidar according to the relevant vehicle applications. In *Laser Radar Technology and Applications XXIV*, Vol. 11005. SPIE, 133–142.

[6] Yalong Hai, Zhongji Yan, Anning Pang, Chenxu Liu, and Anhong Dang. 2023. Immunity to Mutual Interference in Coded Phase-Shift LiDAR. *Journal of Lightwave Technology* 41, 2 (Jan. 2023), 570–577. Conference Name: Journal of Lightwave Technology.

[7] Marcus Hebel, Marcus Hammer, Michael Arens, and Axel L. Diehm. 2018. Mitigation of crosstalk effects in multi-LiDAR configurations. In *Electro-Optical Remote Sensing XII*, Gary Kamerman and Ove Steinvall (Eds.). SPIE, Berlin, Germany, 3.

[8] Gunzung Kim, Jeongsook Eom, and Yongwan Park. 2018. Design of pulsed scanning lidar without mutual interferences. In *Smart Photonic and Optoelectronic Integrated Circuits XX*, Vol. 10536. SPIE, 168–173.

[9] Tianxing Li, Chuankai An, Zhao Tian, Andrew T. Campbell, and Xia Zhou. 2015. Human Sensing Using Visible Light Communication. In *Proceedings of the 21st Annual International Conference on Mobile Computing and Networking (MobiCom '15)*. New York, NY, USA, 331–344.

[10] Jie Xiong and Kyle Jamieson. 2013. ArrayTrack: A Fine-Grained Indoor Location System. In *10th USENIX Symposium on Networked Systems Design and Implementation (NSDI 13)*. USENIX Association, Lombard, IL, 71–84.

[11] Haidong Yan, Jun Li, and Guisheng Liao. 2007. Multitarget identification and localization using bistatic MIMO radar systems. *EURASIP Journal on Advances in Signal Processing* 2008 (2007), 1–8.

[12] Alphan Şahin, Yusuf Said Eroğlu, İsmail Güvenç, Nezih Pala, and Murat Yüksel. 2015. Hybrid 3-D Localization for Visible Light Communication Systems. *Journal of Lightwave Technology* 33, 22 (2015), 4589–4599.